Atmos. Chem. Phys. Discuss., 15, 24369–24401, 2015
www.atmos-chem-phys-discuss.net/15/24369/2015/
doi:10.5194/acpd-15-24369-2015

Atmospheric Chemistry and Physics Discussions

Mixing state, composition, and sources of fine aerosol particles in the Qinghai-Tibetan Plateau and the influence of agricultural biomass burning

W. J. Li[1], S. R. Chen[1], Y. S. Xu[2], X. C. Guo[1,2], Y. L. Sun[3], X. Y. Yang[2], Z. F. Wang[3], X. D. Zhao[4], J. M. Chen[1], and W. X. Wang[1,2]

[1]Environment Research Institute, Shandong University, 250100, Jinan, China
[2]Chinese Research Academy of Environmental Sciences, Beijing 100012, China
[3]State Key Laboratory of Atmospheric Boundary Layer Physics and Atmospheric Chemistry, Institute of Atmospheric Physics, Chinese Academy of Sciences, Beijing 100029, China
[4]Qinghai Environmental Monitoring Center, Qinghai 810007, China

Received: 16 June 2015 – Accepted: 26 August 2015 – Published: 8 September 2015

Correspondence to: W. J. Li (liweijun@sdu.edu.cn) and J. M. Chen (jmchen@sdu.edu.cn)

Published by Copernicus Publications on behalf of the European Geosciences Union.

Abstract

Transmission electron microscopy (TEM) was employed to obtain morphology, size, composition, and mixing state of background fine particles with diameter less than 1 µm in the Qinghai-Tibetan Plateau (QTP) during 15 September to 15 October 2013. Individual aerosol particles mainly contained secondary inorganic aerosols (SIA-sulfate and nitrate) and organics during clean periods ($PM_{2.5}$: particles less than 2.5 µg m^{-3}). The presence of KCl-NaCl associated with organics and an increase of soot particles suggest that an intense biomass burning event caused the highest $PM_{2.5}$ concentrations (> 30 µg m^{-3}) during the study. A large number fraction of the fly ash-containing particles (21.73 %) suggests that coal combustion emissions in the QTP significantly contributed to air pollutants at the median pollution level ($PM_{2.5}$: 10–30 µg m^{-3}). We concluded that emissions from biomass burning and from coal combustion both constantly contribute to anthropogenic particles in the QTP atmosphere. Based on size distributions of individual particles in different pollution levels, we found that gas condensation on existing particles is an important chemical process for the formation of SIA with organic coating. TEM observations show that refractory aerosols (e.g., soot, fly ash, and visible organic particles) likely adhere to the surface of SIA particles larger than 200 nm due to coagulation. Organic coating and soot on surface of the aged particles likely influence their hygroscopic and optical properties in the QTP, respectively. To our knowledge, this study reports the first microscopic analysis of fine particles in the background QTP air.

1 Introduction

With an immense area (about 2 400 000 km^2) and mean elevation of more than 4000 m a.s.l., the Tibetan Plateau (TP), called the "ridge of the world and third polar", plays a key role in Asian climatology, especially the formation of monsoons (Lau et al., 2006). Climate on the TP has warmed 0.3 °C decade^{-1} over the past three

ACPD
15, 24369–24401, 2015

decades, which is twice the rate of observed global warming (Xu et al., 2009). Anthropogenic aerosols and their ice and cloud condensation nuclei (CCN) directly or indirectly leaded to the brightening and diming phenomenon before and after the 1980s in the TP (You et al., 2010). However, light absorbing carbonaceous aerosol particles (i.e., black carbon (BC) and brown carbon (BrC)) can warm the troposphere (Ramanathan and Carmichael, 2008) and accelerate glacier retreat (Xu et al., 2009). Both the radiative effects of aerosols and their role in cloud forming processes depend on their number, size, chemical properties, and mixing state.

As a consequence, a better understanding of climate change can be achieved by characterizing the TP aerosols. Few aerosol measurements have been conducted in the TP. Ion composition records from a shallow ice core (Zheng et al., 2010) and black soot in the Tibetan glaciers (Xu et al., 2009) both showed that anthropogenic aerosols have increased significantly in the most recent 50 years in the TP. Li et al. (2013) obtained aerosol components such as 61 % mineral, 3 % ammonium, 4 % nitrate, 18 % sulfate, 2 % black carbon, and 12 % organic matter in $PM_{2.5}$ at a concentration of 21.5 $\mu g\,m^{-3}$ during summer of 2010 at Qinghai Lake (36°59′ N, 99°54′ E; 3200 m a.s.l.) in the northeastern part of the TP. Coal burning and biomass burning were the major sources for anthropogenic aerosols. Xu et al. (2014) showed that the $PM_{2.5}$ mass concentration of $9.5 \pm 5.4\,\mu g\,m^{-3}$ during a year-long study at the Qilian Shan Station (39.50° N, 96.51° E; 4180 m a.s.l.), a remote site on the northeast edge of the Tibetan Plateau, and their water soluble ionic species were dominated by SO_4^{2-} (39 %), CO_3^{2-} (19 %), Ca^{2+} (16 %), NO_3^- (10 %), and NH_4^+ (6 %). The study suggests anthropogenic aerosol and natural mineral dust from the Gobi desert together contribute to the particle loading in this remote air. Li et al. (2007) also found anthropogenic ions from residential combustion emissions in precipitation samples at Nam Co station of the central TP. In addition, long-range transport of pollutants from eastern and northwestern China and northern India can contribute black carbon and other air pollutants to the TP region (Cao et al., 2010; Wang et al., 2010; Engling et al., 2011; Kopacz et al., 2011; Lu et al., 2012; Xu et al., 2013; Zhao et al., 2013; Cong et al., 2015; Duo et al.,

ACPD
15, 24369–24401, 2015

2015). Although anthropogenic sources make but a minor contribution to the background TP atmosphere, these anthropogenic aerosols significantly enhanced aerosol optical properties (AOD) in the central and northeastern TP in summer (Cong et al., 2009b; Che et al., 2011; Xia et al., 2011). Therefore, study of the composition and sources of aerosol particles in the TP is necessary to understand their effects on the optical, CCN or IN activity.

The TP has various geographic and natural environmental ecosystems such as mountains, lake basins, deserts, forests, and grasslands. Previous sampling sites have included mountain forests, lake basins, and urban areas in the TP (Li et al., 2007; Che et al., 2011; Engling et al., 2011; Li et al., 2013; Xu et al., 2014). However, aerosols of the vast grasslands of the northern TP have not been studied. In this study, we collected samples at a national station of background atmospheric monitoring (NSBAM) on the top of Moshidaban mountain of Menyuan county in Qinghai province (37°35.370′ N; 101°17.329′ E; elevation: 3295 m), which is within the northern part of the Qinghai-Tibet Plateau (QTP) (Fig. 1). The NSBAM is 180 km north of Qinghai Lake (Li et al., 2013) and 160 km from Waliguan station (Che et al., 2011). Only a few herdsmen live in the grassland but many agricultural activities (e.g., growing hulless barley and rape) mainly occur around Qinghai Lake and Menyuan County. Highly aged aerosols after long range transport are of particular interest and represent the typical chemical composition of this continental global background region.

Although many atmospheric scientists have commented on the probable aerosol impacts on climate and monsoon (Lau et al., 2006), atmospheric observations are still very limited because of the unique geographic and natural environment, electric supply problems, high maintenance costs for instruments, and lack of skilled operators. Because of the immensity of the TP, these previous studies, quite scattered in diverse locations, are insufficient to adequately characterize the aerosols throughout this vast region. In addition, the mixing state of individual particles has not been examined, and only a few studies of particle types and soot have been conducted through electron microcopy (D. Zhang et al., 2001; Cong et al., 2009a). Understanding the mixing state

ACPD
15, 24369–24401, 2015

of individual particles sheds light on their source, ageing processes, optical, and hygroscopic properties (Posfai and Buseck, 2010; Li et al., 2015). In the present study, high-resolution transmission electron microscopy (TEM) is employed to study the mixing state and composition of individual fine particles with diameters < 1 µm. The pollution levels have been evaluated and identified through continuous gaseous and particulate instruments at the sampling site. The anthropogenic sources were further identified based on particle types in the QTP.

2 Experimental methods

2.1 Aerosol sampling

Aerosol particles were also collected onto copper TEM grids coated with carbon film (carbon type-B, 300-mesh copper, Tianld Co., China) by a two-stage impactor with a 1-mm-diameter jet nozzle and a 0.5-mm-diameter jet nozzle and an air flow of 1.0 L min^{-1}. Both stages have a 50 % collection efficiency, the first at 0.80 µm and the second at 0.20 µm, with an atmospheric pressure of 69 kpa, a temperature of 283.5 K, and an assumed particle density of 2 g cm^{-3}. Sampling times varied from 30 s to 15 min, depending on particle loading. After collection, each sample was placed in a sealed, dry plastic tube and stored in a desiccator at 25 °C and 20 ± 3 % RH to minimize exposure to ambient air and preserve it for analysis. Altogether, 70 individual samples were collected at the NABAM, of which we analyzed the fine particles collected on only the second stage.

2.2 Individual particle analysis

21 aerosol particle samples collected on TEM grids were analyzed with a JEOL JEM-2100 TEM operated at 200 kV. The details about the aerosol samples were marked in Fig. 3. Elemental composition was determined semi-quantitatively by using an energy-dispersive X-ray spectrometer (EDS) that can detect elements heavier than C. Cu was

ACPD
15, 24369–24401, 2015

excluded from the analyses because the TEM grids are made of Cu. The distribution of aerosol particles on TEM grids was not uniform, with coarser particles occurring near the center and finer particles occurring on the periphery. Therefore, to ensure that the analyzed particles were representative, five areas were chosen from the center and periphery of the sampling spot on each grid. Every particle in the selected area was analyzed. EDS spectra were collected for 15 s in order to minimize radiation exposure and potential beam damage. To better understand the properties of internally mixed aerosol particles, we also analyzed the composition of different components of individual particles, such as coatings, inclusions, and aggregations. The sampling was controlled to avoid coagulation on the substrate during sampling. The projected areas of individual particles were determined by the iTEM software (Olympus soft imaging solutions GmbH, Germany), the standard image analysis platform for electron microscopy. Altogether 4218 particles in these samples were measured for statistical analyses.

2.3 Particle size measurement

Atomic force microscopy (AFM) with a tapping mode analyzed aerosol particles under ambient conditions. AFM, a digital NanoscopeIIIa Instrument, can detect the three-dimensional morphology of particles. The AFM settings contain imaging forces between 1 and 1.5 nN, scanning rates between 0.5 and 0.8 Hz, and scanning range sizes at 10 µm with a resolution of 512 pixels per length. After the AFM analysis, composition of the same particles was confirmed by TEM, with 194 fine aerosol particles analyzed by this method. The NanoScope analysis software can automatically obtain bearing area (A) and bearing volume (V) of each analyzed particle according to the following formula.

$$A = \frac{4}{3}\pi r^2 = \frac{\pi d^2}{3} \rightarrow d = \sqrt{\frac{3A}{\pi}} \quad (1)$$

$$V = \frac{4}{3}\pi r^3 = \frac{4}{3} \times \frac{\pi D^3}{8} \rightarrow D = \sqrt[3]{\frac{6V}{\pi}} \quad (2)$$

ACPD
15, 24369–24401, 2015

Where d is the equivalent circle diameter (ECD) and D the equivalent spherical diameter (ESD). Additionally we know the relation between d and D is $D = 0.64 \times d$, as shown in Fig. 2. As a result, equivalent circle diameters (d) of individual aerosol particles measured from the iTEM software can be further converted into equivalent spherical diameter (D) based on this relationship. In this study, we only considered fine aerosol particles with equivalent spherical diameter smaller than 1 µm.

2.4 FLEXPART particle dispersion model

Air mass history was determined using the Lagrangian particle dispersion model FLEXPART (version 9.02; Stohl et al., 1998). FLEXPART simulates the release of thousands of passive tracer air parcels at the specific location, advecting them backwards in time, providing a representation of the spatial distribution of the air mass at an upwind time referred to as a "retroplume". FLEXPART was driven with 6 h meteorology data from NCEP Climate Forecast System Version 2 (NCEP-CFSv2), including land cover, temperature, relative humidity, and three-dimensional wind, in 37 levels with a resolution of 0.5° × 0.5°. In this study, the modeling periods were 72 h each simulations and it simulated 4 times each day (beginning at 00:00, 06:00, 12:00, and 18:00, respectively) from 00:00 UTC 10 September 2013 to 00:00 UTC 16 October 2013. Every simulation containing 10 000 particles released at the beginning over an altitude range of 3395 to 3995 m a.s.l. and the model outputs were recorded every 3 h. The output data of each simulation were combined together to make the Fig. 1.

2.5 $PM_{2.5}$, trace gases, BC, and meteorological measurements

Thermo TEOM 1405 $PM_{2.5}$ and PM_{10} continually measure the particulate mass concentrations in one-hour averages. Gaseous air pollutants were measured continuously from 1 September to 15 October 2013: O_3 by a UV photometric analyzer (Teledyne Instruments, Model 400EU); SO_2 by a pulsed UV fluorescence analyzer (M100EU), CO by a non-dispersive infrared analyzer (M300EU), and NO and NO_2 by a commer-

ACPD
15, 24369–24401, 2015

cial chemiluminescence analyzer (M200EU), with the concentrations being recorded in five-minute averages. BC concentrations were measured by an Aethalometer and were recorded in one hour averages. In addition, the non-refractory submicron aerosol species including organics, sulfate, nitrate, ammonium, and chloride were measured in-situ by an Aerodyne Aerosol Chemical Speciation Monitor (ACSM) (Du et al., 2015). Wind direction, wind speed, relative humidity (RH), and temperature were measured and recorded in one hour averages. The time-series meteorological data, shown in Fig. S1, and the $PM_{2.5}$ and gaseous concentrations, were provided by the NSBAM.

The average CO mixing ratio is 44.78 ppb at the NSBAM, much lower than the 149 ppb at Waliguan in the summer of 2006, is the site of the observation station of the World Meteorological Organization's (WMO) Global Atmospheric Watch (GAW) (Xue et al., 2011). This contrast shows that the NSBAM adequately represents background conditions in the expansive grasslands of the northern TP. Time-series concentration variations of six pollutants (i.e., $PM_{2.5}$, BC, SO_2, NO_x, CO, and O_3) show that their highest concentrations occurred from 15 to 25 September 2013, and from 11 to 15 October 2013, (Fig. 3). Therefore, we considered these two periods as typical high-pollution events. Table 1 shows that five pollutants' concentrations (i.e., $PM_{2.5}$, BC, SO_2, NO_x, and CO) were higher during these pollution events than in the intervening cleaner period; O_3 concentration was close. When the combustion-tracing CO and NO_x concentrations increase, O_3 mixing ratios generally decrease in the QTP due to photochemical consumption (Xue et al., 2011). The primary BC concentrations during the two pollution events were 17 and 81 % higher than the intervening cleaner period, respectively (Table 1). $PM_{2.5}$ concentration at 17.06 $\mu g\,m^{-3}$ at the NSBAM is slighter lower than the 21.5 $\mu g\,m^{-3}$ in the cleaner Qinghai lake area in the summer of 2010 (Li et al., 2013). The air mass back trajectories during the sampling period commonly came from the northwestern TP and crossed the Qinghai-lake area into the northern TP (Fig. 1). The air masses during the pollution events adequately represented highly aged and processed long-range transported ambient aerosols in the TP. Figure 3 further displays aerosol collection time under three different $PM_{2.5}$ levels, e.g.,

ACPD
15, 24369–24401, 2015

$PM_{2.5} \geq 30\,\mu g\,m^{-3}$, $PM_{2.5}$ between 10 and $30\,\mu g\,m^{-3}$, $PM_{2.5} < 10\,\mu g\,m^{-3}$, which represent high pollution level, medium pollution level, and clean pollution level.

3 Results

3.1 Major fine aerosol particles and mixing states

Based on elemental composition and morphology, aerosol particles were classified into six major categories: mineral dust, KCl-NaCl, fly ash, secondary inorganic aerosol (SIA) containing ammoniated sulfates and nitrates, organics, soot (i.e., BC) (Figs. 4–5). This detailed particle classification scheme is described in our previous studies (Li et al., 2014b, 2015). The nanosized metal particles which have been frequently detected in ambient aerosols in East China (Li et al., 2013a, b) were absent in the Qinghai-Tibet plateau. Mixing properties among the six types of particles were characterized in detail because understanding their mixing state enables one to determine their sources, optical properties, hygroscopic behavior, related heterogeneous reactions, and potential health effects (Li et al., 2015). TEM observations indicate that SIA and organics coexisted in individual fine particles and that organic carbon (OC) normally coated these SIA particles (e.g., Figs. 4d, 5a, and 6). In addition, we found that many SIA-OC particles had visible inclusions such as mineral dust, fly ash, organic carbon, and soot particles. Identification of the refractory inclusions in internally mixed particles enables one to trace particle sources and their history in the aging air mass. Their mixing properties consist mostly of SIA-soot-OC (e.g., Fig. 4c), SIA-fly ash-soot (e.g., Fig. 5d), SIA-fly ash-OC (visible) (e.g., Fig. 5d), SIA-fly ash (e.g., Fig. 5c), SIA-mineral, SIA-visible OC (e.g., Fig. 5a). Therefore, SIA and OC in aerosol particles in the Qinghai-Tibet Plateau were the two most important influences of the mixing state of primary particles.

ACPD
15, 24369–24401, 2015

3.2 Size distribution of aerosol particles

In this section, we describe the size distribution of individual particles with their diameters from 40 nm to 1 µm in different pollution levels. 684 particles collected during clean periods show a median diameter of 230 nm. Figure 7a shows that the size distribution of particles without inclusions determines ambient particle size.

1214 particles during high pollution levels have a median diameter of 260 nm (Fig. 7b). Particles with inclusions and particles without inclusions have median diameters of 300 and 230 nm, respectively. Figure 7b shows particles with and without inclusions jointly determine the particle size distribution during high pollution levels. We noticed that the size distribution of inclusions in SIA displays a median diameter of 150 nm. A similar pattern of size distribution of 2355 particles occurred in median pollution levels (Fig. 7c). The median diameters of total individual particles, particles with inclusions, particle without inclusions, and inclusions are 290, 340, 250, and 150 nm, respectively. Therefore, the inclusions (e.g., mineral, fly ash, soot, and spherical organic particles) significantly enhanced particle sizes in the background air once they were internally mixed with sulfates.

4 Discussion

4.1 Identification of the pollution events

TEM observations show that individual particle types display large differences under three different $PM_{2.5}$ levels: $\geq 30\,\mu g\,m^{-3}$ (high pollution level), 10–30 $\mu g\,m^{-3}$ (medium pollution level), and $< 10\,\mu g\,m^{-3}$ (clean pollution level) (Fig. 3). Aerosol particles collected in clean periods mainly contained SIA and organics. Figure 6 shows that individual SIA particles were commonly coated by organics. Consistently, the ACSM measurement showed that SO_4^{2-} and organics were the main components in PM_1, accounting for 33–36 and 34–48 % at the sampling site, respectively (Du et al., 2015).

ACPD
15, 24369–24401, 2015

Figure 8 presents the composition of all the analyzed individual particles in the three pollution levels. In the clean period, we found only a few anthropogenic particles such as fly ash, soot, or their mixed particles with their contributions being less than 10 % (Fig. 8a).

The increase of KCl and soot particles is suggestive of an intense biomass burning event at the background site (Li et al., 2003). In this study, abundant KCl-NaCl particles and soot-containing particles (e.g., Fig. 4) only occurred in pollution period 1 and period 2 which have been indicated as biomass burning (Du et al., 2015). Because KCl-NaCl particles associated with organic matter distributed lower than 1 µm and only occurred in short period, they should be excluded from the possible natural sources such as saline Qinghai Lake and desert. In addition, our field experimental investigations showed that a few farmers burned cole flowers and highland barley during the autumn harvest season, which are main season crops in the QTP. In addition, the burning of cow dung for residential heating likely caused the high $PM_{2.5}$ in 11–15 October (Du et al., 2015).

The distribution of different particle types in the medium pollution level is similar to the high pollution level, except for the absence of KCl-NaCl particles. Figure 8c shows that a large amount of fly ash-containing particles occurred in medium pollution level. Fly ash is generally considered as a reliable fingerprint of coal combustion in residential cooking, power plants, and industrial activities (Li and Shao, 2009). The fly ash-containing particles increase from 11.40 % in the high pollution level to 21.73 % in the medium one, but soot-containing particles decrease from 38.40 to 25.87 %. This result indicates that coal combustion emissions in the QTP significantly affected the background air quality. Compared to individual particles in polluted East China, absence of nanometer metal particles in the QTP suggests that there are no large heavy metal-related industrial emissions in the area under air mass back trajectories (Fig. 1). The China Energy Statistical Yearbook of 2013 shows coal combustion occurs in power plants (48.5 %), heavy industries (36.4 %), and house cooking/heating in rural areas (8.6 %) in Qinghai province, particularly nearby the large cities such as Xi'ning (Wen

ACPD
15, 24369–24401, 2015

et al., 2013). Although we did not find any KCl-NaCl particle in the samples under median pollution level, 50 % of SIA (OC coating) and SIA-soot particles containing minor K (Fig. 4c and d) frequently occurred in the samples. During long-range transport, once coagulation and condensation of ammoniated sulfates and sulfuric acid in biomass burning particles increase, K-rich particles may transform into sulfur-rich particles with certain amounts of K (Li et al., 2014b). Therefore, SIA particles containing minor K suggest that biomass burning emissions likely contributed to the QTP aerosols on a more or less constant basis. A similar result has been obtained through the analysis of organic species in $PM_{2.5}$ at Qinghai-lake (Li et al., 2013). Therefore, we conclude that emissions from biomass burning and from coal combustion significantly contribute to the formation of anthropogenic fine particles in the atmosphere over the QTP.

4.2 Regional effects of biomass burning and industrial emissions

The previous studies proved that trace gases such as SO_2, NO_x, and volatile organic compounds (VOCs) from anthropogenic and natural sources had been transported long distances in the QTP and were transformed into secondary aerosol particles (Xue et al., 2011; Li et al., 2013; Du et al., 2015; Xu et al., 2015). For example, Du et al. (2015) suggested that secondary sulfates and oxygenated organic aerosols from anthropogenic sources and biomass burning displayed a regional property in the QTP. Because of measurement limitations, there is no research about refractory aerosol particles (e.g., mineral, fly ash, soot, and primary organic particles) in fine particles. In contrast, TEM observations can adequately characterize these refractory particles internally mixed with SIA based on their unique morphology and composition (Figs. 4 and 5). We identified abundant refractory particles at the three pollution levels at the regional background site. Therefore, the nanosized refractory particles and trace gases from various anthropogenic sources including biomass burning can together be transported long distances. The FLEXPART simulation shows that these anthropogenic particles mainly originated from biomass burning between the Qinghai lake and Menyuan

ACPD
15, 24369–24401, 2015

county and heavy industries and coal-fired power plants in western areas of Xining city (Fig. 1).

4.3 Mixing mechanisms of aged aerosol particles

The results show that more than 90 % of particles at the background site were highly aged. SIA with OC coating were the dominant particles and determined the hygroscopic properties of the ambient aerosol particles. Organic coatings on inorganic particles can induce an early deliquescence of particle surface compared to that of the pure inorganic compounds (Li et al., 2014a). Recently, Mikhailov et al. (2015) found that the semi-solid state of the organic coating can lead to kinetic limitations of water uptake and release during hydrate and dehydrate cycles in the background area. Organics dominated in fine particles, accounting for 43 % of mass on average, followed by sulfate (28 %) and nitrate (1 %) (Du et al., 2015). TEM observations further indicated that organics can heterogeneously and homogeneously be mixed with all the fine SIA particles (Figs. 6, 9, and 10). This finding is in agreement with the study of new particle formation and growth events during the sampling period, in which oxygenated organics significantly contributed into particle growth in the QTP (Du et al., 2015). Figure 7 shows that SIA with OC coating shift to one smaller size than the total individual particles. Gas condensation on the existing particles is an important chemical process for formation of SIA with OC coating. Therefore, organic coating of the aged aerosol particles is likely an important factor to determine particle hygroscopic growth and phase transitions in the QTP.

Inclusions within SIA particles increase their size by 36–42 % (Fig. 8). The size distribution of individual particles shows that particles without inclusions have a median size of 200–250 nm at the background site. Figure 8 shows that the number of particles with inclusions increases substantially with diameters above 200 nm. In addition, Figs. 9 and 10 show soot, fly ash, and visible organic particles likely adhere to the surface of SIA particles, which is different from many refractory particles embedded within SIA particles in East China (Li and Shao, 2009; Li et al., 2011b, 2014b). Therefore, the

ACPD
15, 24369–24401, 2015

coagulation process between primary refractory particles and SIA particles with diameters > 200 nm could be dominant in the atmosphere. The results are different from the background aerosol particles in Siberia where these soot, fly ash and visible organic particles are absent (Mikhailov et al., 2015). In particular, the mixing structure of soot on the surface of SIA particles is different from the previous studies (Li et al., 2003; Adachi et al., 2010; Li et al., 2015). Therefore, sulfates cannot act as the lens to enhance optical absorption of soot particles before individual particles totally deliquesces in humid air (Ramanathan and Carmichael, 2008). Light absorption of soot on surfaces of sulfate particles have 30 % lower than soot centered within sulfate particles (Adachi et al., 2010). We found that number of soot-containing particles increase during the biomass burning periods (Fig. 8b and c). Also, Fig. 3 shows that the BC concentrations exceeded 1.0 $\mu g\,m^{-3}$ during biomass burning periods which is two times higher than the average value during the sampling period. As a result, large amounts of soot particles from biomass burning in background atmosphere likely change atmospheric optical absorption and modify optical feedback of ice/snow after their deposition in the QTP (Che et al., 2011; Ming et al., 2012). The microstructure of soot particles can improve understanding of the optical properties of fine aerosol particles and better evaluate their climate impacts using climate models.

We also notice that a large number of particles without inclusions can occur with diameters > 300 nm, although the particle numbers decrease (Fig. 7). TEM observations reveal distinct rims on some larger particles, as the examples shown in Figs. 5a, 5d, 9b, 10a. Our previous studies showed that the cloud and fog residues on the substrate can display distinct rims (Kojima et al., 2004; Li et al., 2011a, b). Therefore, these large particles with distinct rims probably undergo complicated atmospheric transformation such as cloud/fog processing during their growth. Briefly, our study indicates that aerosol particles in different size regimes have different atmospheric chemical or physical processes in the background air over the QTP.

ACPD
15, 24369–24401, 2015

4.4 Further considerations about fine particles over Qinghai-Tibetan plateau

Emissions from coal combustion and biomass burning contribute fine particles into the background air over the QTP. Because of the sensitive feedback of climate in the TP, the highly aged aerosol particles in the plateau become particularly interesting. Firstly, transport and sources of aerosol particles should be evaluated, and, indeed, most studies in the TP have accomplished this (Cong et al., 2009a, b; Engling et al., 2011; Lu et al., 2012; Du et al., 2015; Xu et al., 2015). These studies all suggested that long-range transport of fine particles from biomass burning and other anthropogenic sources (cooking and vehicular emissions) often reach the TP. However, the emissions of coal combustion from power plants or other industrial sources have a decided regional influence has not been reported. Our studies provide new evidence that fly ash particles serve as a reliable fingerprint of coal-combustion at the background site. Following economic development in western China, coal combustion increases, chiefly for electrical power generation and other industrial activities (Fig. S2). Secondly, highly aged particles such as ambient aerosols and CCN in the atmosphere and sediment in ice/snow can directly or indirectly impact on climate in the TP (Cong et al., 2009b; You et al., 2010; Che et al., 2011; Lu et al., 2012; Ming et al., 2012; He et al., 2014; Wang et al., 2015; Yang et al., 2015). At the background sampling site the mean BC concentration was 0.54 $\mu g\,m^{-3}$. Interestingly, we found that most fine soot (BC) particles adhere to individual SIA (Figs. 9 and 10) in the Qinghai plateau while many soot particles were embedded within SIA in polluted areas of East China (Li and Shao, 2009; Li et al., 2011b). The detailed physical properties (e.g., mixing structure and size) of soot in air and ice/snow should be further studied in the TP, which can improve the current climate models. Thirdly, the dominant organics, sulfates, and minor nitrates in fine aerosol particles in the TP are largely different from their counterparts in more polluted areas (Li et al., 2013; Du et al., 2015; Xu et al., 2015), where have high organics, sulfate and nitrate in fine particles. Although regional transport from anthropogenic sources or biomass burning significantly increase particle concentrations,

ACPD
15, 24369–24401, 2015

mineral dust from surrounding deserts and organics from plants are still dominant in the TP throughout the year (X. Y. Zhang et al., 2001; Wang et al., 2010; Li et al., 2013; Xu et al., 2014). Fourthly, the high-elevation TP with its unique climatic features and special sources of aerosol particles and trace gases could lead to a different type of atmospheric chemistry. Therefore, it is important to understand how this somewhat different atmospheric chemistry is related to the climate in this background atmosphere (Li et al., 2015). Features of this altered atmospheric chemistry include new particle formation and growth (Du et al., 2015), the mixing state of soot (BC) (D. Zhang et al., 2001; Cong et al., 2009a), heterogeneous reactions on surfaces of mineral particles (Xu et al., 2015), and the mixing state, formation, and species of organic aerosols (Xu et al., 2013; Du et al., 2015; Xu et al., 2015). Atmospheric chemistry in the pristine atmosphere would most likely differ from that in the polluted air of East China. However, current knowledge is insufficient to understand particle ageing and formation in the TP.

5 Conclusions

Time-series of six pollutants ($PM_{2.5}$, BC, SO_2, NO_x, CO, and O_3) were obtained at a national station of background atmospheric monitoring (NSBAM) on the top of Moshidaban Mountain in the QTP during 15 September–15 October 2013. The mean concentrations of $PM_{2.5}$, BC, SO_2, NO_x, CO, and O_3 were 17.06 $\mu g\,m^{-3}$, 0.54 $\mu g\,m^{-3}$, 1.27 ppb, 2.05 ppb, 44.78 ppb, and 50.00 ppb, respectively. TEM was employed to study individual fine particles with the diameter less than 1 µm that were classified into six major particle types: mineral dust, KCl-NaCl, fly ash, secondary inorganic aerosol (SIA) containing ammoniated sulfates and nitrates, organics, soot (i.e., BC). Individual fine particle types display large differences under three different $PM_{2.5}$ levels: $PM_{2.5} \geq 30\ \mu g\,m^{-3}$ (high pollution level), $10 \leq PM_{2.5} < 30\ \mu g\,m^{-3}$ (medium pollution level), and $< 10\ \mu g\,m^{-3}$ (clean period). Individual fine particles in clean periods mainly contained SIA and organics. The presence of KCl-NaCl coated by organics and increased soot particles during high pollution levels suggests an intense biomass burning event near the back-

ACPD
15, 24369–24401, 2015

ground site. Large amounts of fly ash-containing particles occurred in medium pollution level. The fly ash-containing particles increased from 11.40 % at the median pollution level to 21.73 % at the high pollution level, but soot-containing particles decreased from 38.40 to 25.87 %. This result indicates that coal combustion emissions in the QTP significantly affected the background air quality. In addition, SIA particles containing minor K suggest that biomass burning emissions were a constant contributor to aerosol particles in the QTP. We concluded that the emissions from biomass burning and coal-used anthropogenic activities contribute anthropogenic particles into the QTP atmosphere.

Aerosol particles containing SIA core and OC coating display smaller medium size than the total particles. Gas condensation on the particles is an important chemical process for their formation. The number concentration of particles with inclusions increased markedly above 200 nm. TEM observations show that refractory aerosols (e.g., soot, fly ash, and visible organic particles) likely adhere to the surface of SIA particles, suggesting physical coagulation could be dominant in background air. These results notably improve our understanding of sources and ageing processes of long-range transported aerosols in the QTP. The transport of these aerosol particles, as well as their, hygroscopic, and optical properties and atmospheric chemistry, require further study in the TP.

The Supplement related to this article is available online at doi:10.5194/acpd-15-24369-2015-supplement.

Author contributions. W. J. Li and J. M. Chen designed the research and wrote the paper; W. J. Li and S. R. Chen carried TEM and AFM experiments; Y. S. Xu, X. C. Guo, Y. L. Sun, and X. Y. Yang conducted field experiments; X. D. Zhao provided the online monitoring data; Y. S. Xu, J. M. Chen, Z. F. Wang, and W. X. Wang lead the projects.

Acknowledgements. We appreciate Peter Hyde's comments and proofreading. We are grateful to Yong Ren for processing FLEXPART data for Fig. 1. This work was supported by the National

ACPD
15, 24369–24401, 2015

Natural Science Foundation of China (41575116 and 41375133), Shandong Provincial Science Fund for Distinguished Young Scholars, China (JQ201413), Young Scholars Program of Shandong University (2015WLJH37), Taishan Scholars (ts20120522), Fundamental Research Funds of Shandong University (2014QY001), and State Key Laboratory of Atmospheric Boundary Layer Physics and Atmospheric Chemistry (LAPC-KF-2014–03).

References

Adachi, K., Chung, S. H., and Buseck, P. R.: Shapes of soot aerosol particles and implications for their effects on climate, J. Geophys. Res., 115, D15206, doi:10.1029/2009JD012868, 2010.

Cao, J., Tie, X., Xu, B., Zhao, Z., Zhu, C., Li, G., and Liu, S.: Measuring and modeling black carbon (BC) contamination in the SE Tibetan Plateau, J. Atmos. Chem., 67, 45–60, 2010.

Che, H., Wang, Y., and Sun, J.: Aerosol optical properties at Mt. Waliguan Observatory, China, Atmos. Environ., 45, 6004–6009, 2011.

Cong, Z., Kang, S., Dong, S., and Zhang, Y.: Individual particle analysis of atmospheric aerosols at Nam Co, Tibetan Plateau, Aerosol Air Qual. Res., 9, 323–331, 2009a.

Cong, Z., Kang, S., Smirnov, A., and Holben, B.: Aerosol optical properties at Nam Co, a remote site in central Tibetan Plateau, Atmos. Res., 92, 42–48, 2009b.

Cong, Z., Kawamura, K., Kang, S., and Fu, P.: Penetration of biomass-burning emissions from South Asia through the Himalayas: new insights from atmospheric organic acids, Sci. Rep., 5, doi:10.1038/srep09580, 2015.

Du, W., Sun, Y. L., Xu, Y. S., Jiang, Q., Wang, Q. Q., Yang, W., Wang, F., Bai, Z. P., Zhao, X. D., and Yang, Y. C.: Chemical characterization of submicron aerosol and particle growth events at a national background site (3295 m a.s.l.) in the Tibetan Plateau, Atmos. Chem. Phys. Discuss., 15, 13515–13550, doi:10.5194/acpd-15-13515-2015, 2015.

Duo, B., Zhang, Y., Kong, L., Fu, H., Hu, Y., Chen, J., Li, L., and Qiong, A.: Individual particle analysis of aerosols collected at Lhasa City in the Tibetan Plateau, J. Environ. Sci., 29, 165–177, 2015.

Engling, G., Zhang, Y.-N., Chan, C.-Y., Sang, X.-F., Lin, M., Ho, K.-F., Li, Y.-S., Lin, C.-Y., and Lee, J. J.: Characterization and sources of aerosol particles over the southeastern Ti-

ACPD
15, 24369–24401, 2015

betan Plateau during the Southeast Asia biomass-burning season, Tellus B, 63, 117–128, doi:10.1111/j.1600-0889.2010.00512.x, 2011.
He, C., Li, Q., Liou, K.-N., Takano, Y., Gu, Y., Qi, L., Mao, Y., and Leung, L. R.: Black carbon radiative forcing over the Tibetan Plateau, Geophys. Res. Lett., 41, 7806–7813, doi:10.1002/2014GL062191, 2014.
Kojima, T., Buseck, P. R., Wilson, J. C., Reeves, J. M., and Mahoney, M. J.: Aerosol particles from tropical convective systems: cloud tops and cirrus anvils, J. Geophys. Res., 109, 12201–12201, 2004.
Kopacz, M., Mauzerall, D. L., Wang, J., Leibensperger, E. M., Henze, D. K., and Singh, K.: Origin and radiative forcing of black carbon transported to the Himalayas and Tibetan Plateau, Atmos. Chem. Phys., 11, 2837–2852, doi:10.5194/acp-11-2837-2011, 2011.
Lau, K. M., Kim, M. K., and Kim, K. M.: Asian summer monsoon anomalies induced by aerosol direct forcing: the role of the Tibetan Plateau, Clim. Dynam., 26, 855–864, 2006.
Li, C., Kang, S., Zhang, Q., and Kaspari, S.: Major ionic composition of precipitation in the Nam Co region, Central Tibetan Plateau, Atmos. Res., 85, 351–360, 2007.
Li, J., Posfai, M., Hobbs, P. V., and Buseck, P. R.: Individual aerosol particles from biomass burning in southern Africa: 2, Compositions and aging of inorganic particles, J. Geophys. Res., 108, doi:10.1029/2002JD002310, 2003.
Li, J. J., Wang, G. H., Wang, X. M., Cao, J. J., Sun, T., Cheng, C. L., Meng, J. J., Hu, T. F., and Liu, S. X.: Abundance, composition and source of atmospheric $PM_{2.5}$ at a remote site in the Tibetan Plateau, China, Tellus B, 65, doi:10.3402/tellusb.v65i0.20281, 2013.
Li, W., Li, P., Sun, G., Zhou, S., Yuan, Q., and Wang, W.: Cloud residues and interstitial aerosols from non-precipitating clouds over an industrial and urban area in northern China, Atmos. Environ., 45, 2488–2495, 2011.
Li, W., Wang, T., Zhou, S., Lee, S., Huang, Y., Gao, Y., and Wang, W.: Microscopic observation of metal-containing particles from Chinese continental outflow observed from a non-industrial site, Environ. Sci. Technol., 47, 9124–9131, 2013a.
Li, W., Wang, Y., Collett, J. L., Chen, J., Zhang, X., Wang, Z., and Wang, W.: Microscopic evaluation of trace metals in cloud droplets in an acid precipitation region, Environ. Sci. Technol., 47, 4172–4180, 2013b.
Li, W., Chi, J., Shi, Z., Wang, X., Chen, B., Wang, Y., Li, T., Chen, J., Zhang, D., Wang, Z., Shi, C., Liu, L., and Wang, W.: Composition and hygroscopicity of aerosol particles at

ACPD
15, 24369–24401, 2015

Mt. Lu in South China: implications for acid precipitation, Atmos. Environ., 94, 626–636, doi:10.1016/j.atmosenv.2014.06.003, 2014a.

Li, W., Shao, L., Shi, Z., Chen, J., Yang, L., Yuan, Q., Yan, C., Zhang, X., Wang, Y., Sun, J., Zhang, Y., Shen, X., Wang, Z., and Wang, W.: Mixing state and hygroscopicity of dust and haze particles before leaving Asian continent, J. Geophys. Res., 119, 1044–1059, 2014b.

Li, W., Shao, L., Zhang, D., Ro, C.-U., Hu, M., Bi, X., Geng, H., Matsuki, A., Niu, H., and Chen, J.: A review of single aerosol particle studies in the atmosphere of East Asia: morphology, mixing state, source, and heterogeneous reactions, J. Clean. Prod., doi:10.1016/j.jclepro.2015.04.050, online first, 2015.

Li, W. J. and Shao, L. Y.: Transmission electron microscopy study of aerosol particles from the brown hazes in northern China, J. Geophys. Res., 114, D09302, doi:10.1029/2008JD011285, 2009.

Li, W. J., Zhou, S. Z., Wang, X. F., Xu, Z., Yuan, C., Yu, Y. C., Zhang, Q. Z., and Wang, W. X.: Integrated evaluation of aerosols from regional brown hazes over northern China in winter: concentrations, sources, transformation, and mixing states, J. Geophys. Res., 116, D09301, doi:10.1029/2010JD015099, 2011.

Lu, Z., Streets, D. G., Zhang, Q., and Wang, S.: A novel back-trajectory analysis of the origin of black carbon transported to the Himalayas and Tibetan Plateau during 1996–2010, Geophys. Res. Lett., 39, L01809, doi:10.1029/2011gl049903, 2012.

Mikhailov, E. F., Mironov, G. N., Pöhlker, C., Chi, X., Krüger, M. L., Shiraiwa, M., Förster, J.-D., Pöschl, U., Vlasenko, S. S., Ryshkevich, T. I., Weigand, M., Kilcoyne, A. L. D., and Andreae, M. O.: Chemical composition, microstructure, and hygroscopic properties of aerosol particles at the Zotino Tall Tower Observatory (ZOTTO), Siberia, during a summer campaign, Atmos. Chem. Phys., 15, 8847–8869, doi:10.5194/acp-15-8847-2015, 2015.

Ming, J., Du, Z., Xiao, C., Xu, X., and Zhang, D.: Darkening of the mid-Himalaya glaciers since 2000 and the potential causes, Environ. Res. Lett., 7, 014021, doi:10.1088/1748-9326/7/1/014021, 2012.

Posfai, M. and Buseck, P. R.: Nature and climate effects of individual tropospheric aerosol particles, Annu. Rev. Earth Pl. Sc., 38, 17–43, 2010.

Ramanathan, V. and Carmichael, G.: Global and regional climate changes due to black carbon, Nat. Geosci., 1, 221–227, 2008.

ACPD
15, 24369–24401, 2015

Stohl, A., Hittenberger, M., and Wotawa, G.: Validation of the lagrangian particle dispersion model FLEXPART against large-scale tracer experiment data, Atmos. Environ., 32, 4245–4264, doi:10.1016/S1352-2310(98)00184-8, 1998.

Wang, Q. Y., Huang, R.-J., Cao, J. J., Tie, X. X., Ni, H. Y., Zhou, Y. Q., Han, Y. M., Hu, T. F., Zhu, C. S., Feng, T., Li, N., and Li, J. D.: Black carbon aerosol in winter northeastern Qinghai-Tibetan Plateau, China: the effects from South Asia pollution, Atmos. Chem. Phys. Discuss., 15, 14141–14169, doi:10.5194/acpd-15-14141-2015, 2015.

Wang, X., Huang, J., Zhang, R., Chen, B., and Bi, J.: Surface measurements of aerosol properties over northwest China during ARM China 2008 deployment, J. Geophys. Res., 115, doi:10.1029/2009JD013467, 2010.

Wen, J., Meng, H., and Wang, X.: China Energy Statistical Yearbook, Department of Energy Statistics, National Bureau of Statistics, People's Republic of China, Beijing, 1–355, 2013.

Xia, X., Zong, X., Cong, Z., Chen, H., Kang, S., and Wang, P.: Baseline continental aerosol over the central Tibetan plateau and a case study of aerosol transport from South Asia, Atmos. Environ., 45, 7370–7378, 2011.

Xu, B., Cao, J., Hansen, J., Yao, T., Joswia, D. R., Wang, N., Wu, G., Wang, M., Zhao, H., Yang, W., Liu, X., and He, J.: Black soot and the survival of Tibetan glaciers, P. Natl. Acad. Sci. USA, 106, 22114–22118, 2009.

Xu, J., Zhang, Q., Li, X., Ge, X., Xiao, C., Ren, J., and Qin, D.: Dissolved organic matter and inorganic ions in a Central Himalayan glacier – insights into chemical composition and atmospheric sources, Environ. Sci. Technol., 47, 6181–6188, 2013.

Xu, J., Wang, Z., Yu, G., Qin, X., Ren, J., and Qin, D.: Characteristics of water soluble ionic species in fine particles from a high altitude site on the northern boundary of Tibetan Plateau: mixture of mineral dust and anthropogenic aerosol, Atmos. Res., 143, 43–56, 2014.

Xu, J. Z., Zhang, Q., Wang, Z. B., Yu, G. M., Ge, X. L., and Qin, X.: Chemical composition and size distribution of summertime $PM_{2.5}$ at a high altitude remote location in the northeast of the Qinghai–Xizang (Tibet) Plateau: insights into aerosol sources and processing in free troposphere, Atmos. Chem. Phys., 15, 5069–5081, doi:10.5194/acp-15-5069-2015, 2015.

Xue, L. K., Wang, T., Zhang, J. M., Zhang, X. C., Deliger, Poon, C. N., Ding, A. J., Zhou, X. H., Wu, W. S., Tang, J., Zhang, Q. Z., and Wang, W. X.: Source of surface ozone and reactive nitrogen speciation at Mount Waliguan in western China: new insights from the 2006 summer study, J. Geophys. Res., 116, doi:10.1029/2010JD014735, 2011.

ACPD
15, 24369–24401, 2015

Yang, S., Xu, B., Cao, J., Zender, C. S., and Wang, M.: Climate effect of black carbon aerosol in a Tibetan Plateau glacier, Atmos. Environ., 111, 71–78, 2015.
You, Q., Kang, S., Flügel, W.-A., Sanchez-Lorenzo, A., Yan, Y., Huang, J., and Martin-Vide, J.: From brightening to dimming in sunshine duration over the eastern and central Tibetan Plateau (1961–2005), Theor. Appl. Climatol., 101, 445–457, 2010.
Zhang, D., Iwasaka, Y., and Shi, G.: Soot particles and their impacts on the mass cycle in the Tibetan atmosphere, Atmos. Environ., 35, 5883–5894, 2001.
Zhang, X. Y., Arimoto, R., Cao, J. J., An, Z. S., and Wang, D.: Atmospheric dust aerosol over the Tibetan Plateau, J. Geophys. Res., 106, 18471–18476, 2001.
Zhao, Z., Cao, J., Shen, Z., Xu, B., Zhu, C., Chen, L. W. A., Su, X., Liu, S., Han, Y., Wang, G., and Ho, K.: Aerosol particles at a high-altitude site on the Southeast Tibetan Plateau, China: implications for pollution transport from South Asia, J. Geophys. Res., 118, 11360–11375, 2013.
Zheng, W., Yao, T., Joswiak, D. R., Xu, B., Wang, N., and Zhao, H.: Major ions composition records from a shallow ice core on Mt. Tanggula in the central Qinghai-Tibetan Plateau, Atmos. Res., 97, 70–79, 2010.

ACPD
15, 24369–24401, 2015

Table 1. Concentrations of six air pollutants during the sampling period, two pollution periods, and clean period.

Pollutants	All data		Polluted period-1		Polluted period-2		Other period	
	mean	*n*	mean	*n*	mean	*n*	mean	*n*
$PM_{2.5}$ ($\mu g\,m^{-3}$)	17.06	715	17.60	152	24.45	99	15.32	464
BC ($\mu g\,m^{-3}$)	0.54	805	0.55	176	0.85	119	0.47	510
SO_2 (ppb)	1.27	8822	1.21	1981	2.73	1063	1.03	5778
NO_x (ppb)	2.05	8842	2.37	2001	3.41	1063	1.69	5778
CO (ppb)	44.78	7822	63.45	1939	104.23	1030	24.68	4853
O_3 (ppb)	50.00	8817	47.87	2000	49.01	1039	50.53	5778

All data period: 10 September–15 October 2013; Polluted period-1: 18–25 September 2013; Polluted period-2: 11–15 October 2013.

ACPD
15, 24369–24401, 2015

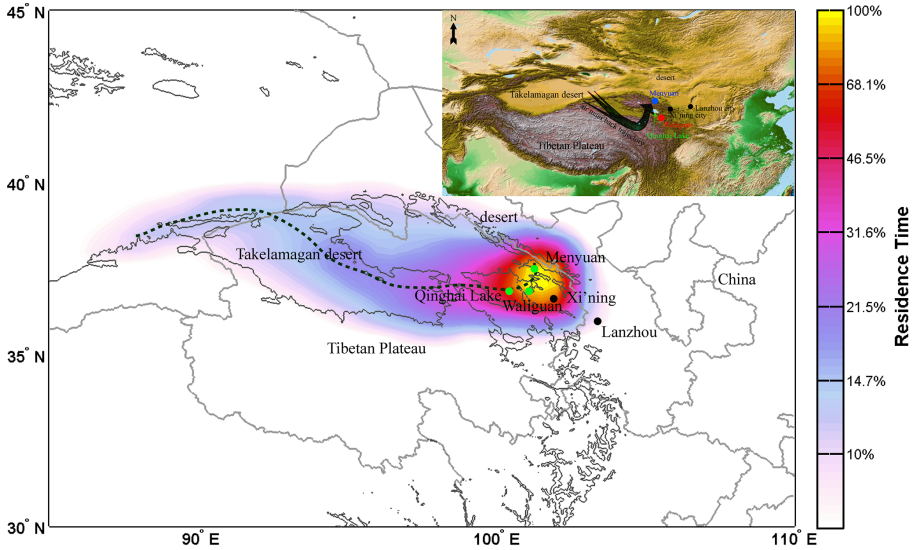

Figure 1. FLEXPART retroplume simulations during 10 September–15 October. Topographical map showing the the sampling location and surrounding regions in the Tibetan Plateau. Xi'ning is the caption city of Qinghai province. Menyuan represents sampling site. The black line shows the major back trajectories of air mass during 10 September–15 October 2013 based on the spatial distribution of the air mass. The main air mass mainly passed through rural areas, grasslands, and desert.

ACPD
15, 24369–24401, 2015

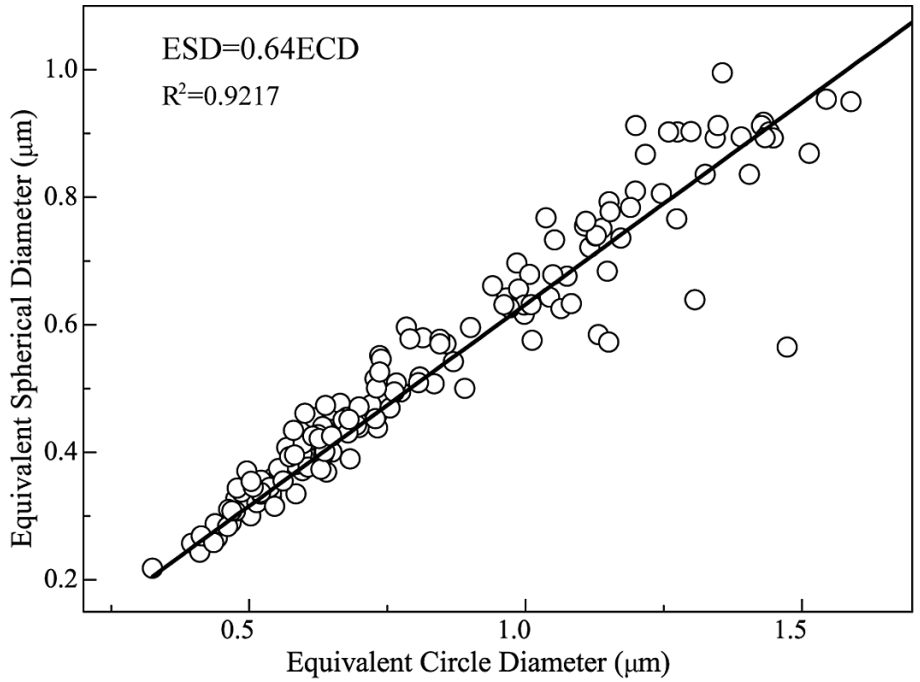

Figure 2. Correction of equivalent circle diameters (ECD) vs. equivalent spherical diameter (ESD) of 157 aerosol particles.

ACPD
15, 24369–24401, 2015

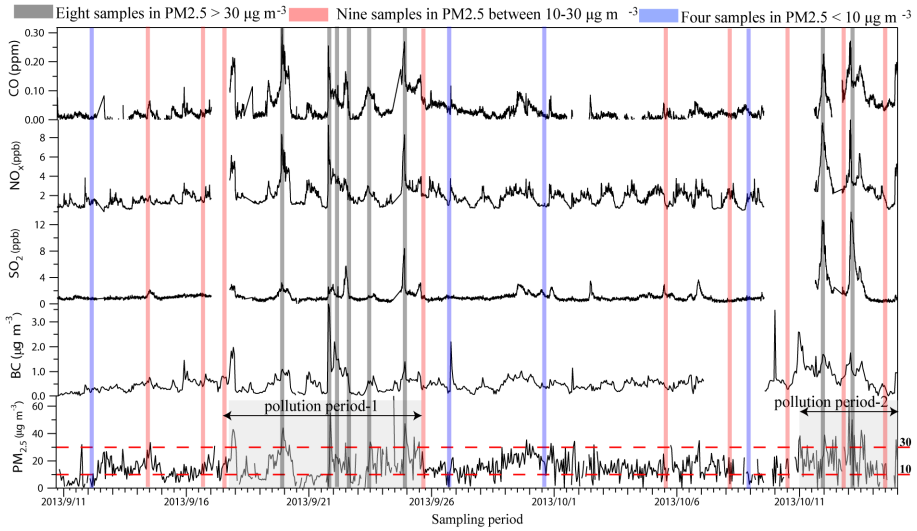

Figure 3. Time-series concentration of air pollutants (i.e., CO, NO_x, SO_2, BC, and $PM_{2.5}$) during 11 September–15 October 2013. The sampling time was marked by grey column ($PM_{2.5} \geq 30\,\mu g\,m^{-3}$), pink column ($PM_{2.5}$ between 10 and $30\,\mu g\,m^{-3}$), blue column ($PM_{2.5} < 10\,\mu g\,m^{-3}$).

ACPD
15, 24369–24401, 2015

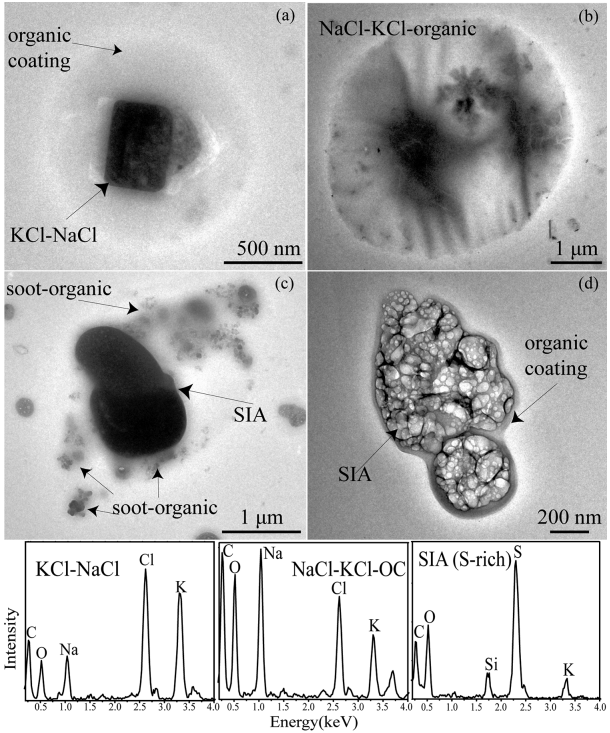

Figure 4. TEM images of **(a, b)** KCl-NaCl particle with organic coating on 22 September and 13 October. **(c)** SIA-soot with organic coating on 22 September. **(d)** SIA with organic coating on 11 October. EDS spectra shows elemental compositions of each particle type in each TEM image.

ACPD
15, 24369–24401, 2015

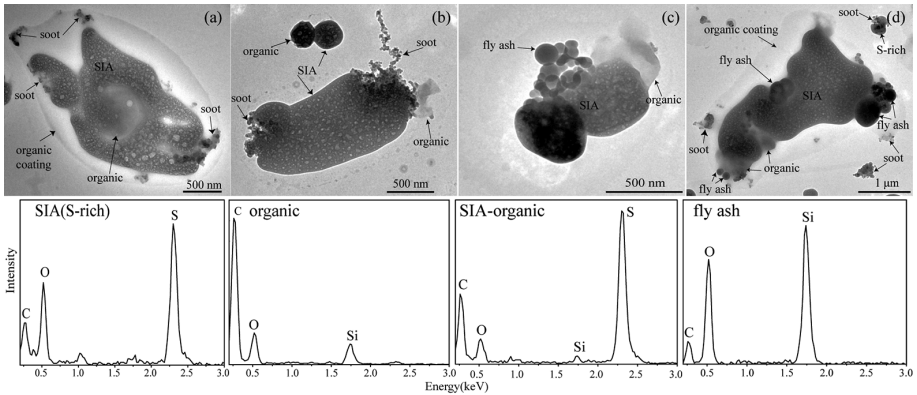

Figure 5. TEM images of **(a)** SIA-soot-OC (visible) with organic coating on 16 September. **(b)** SIA-soot-OC on 14 September. **(c)** SIA-fly ash-OC on 5 October. **(d)** SIA-fly ash-soot-OC (visible) with organic coating on 16 September. EDS spectra shows elemental composition of each particle type in each TEM image.

ACPD
15, 24369–24401, 2015

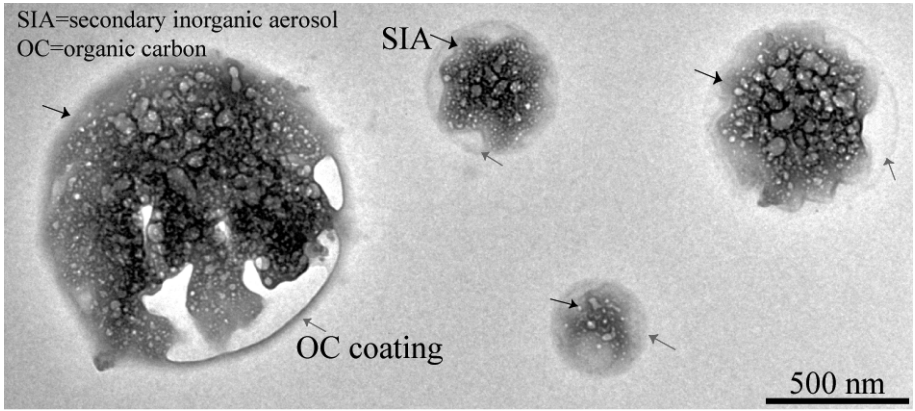

Figure 6. TEM image of individual particles collected in clean period with $PM_{2.5}$ mass concentration less than 10 $\mu g\,m^{-3}$. SIA particles are internally mixed with organics.

ACPD
15, 24369–24401, 2015

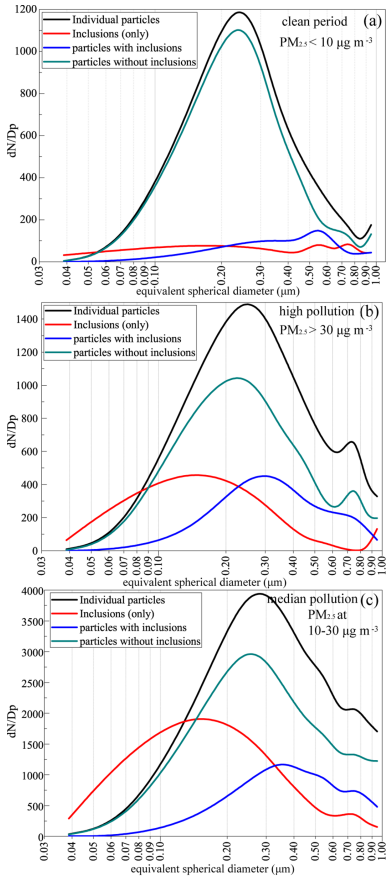

Figure 7. Size distribution of individual particles, inclusions, particles with inclusions, and particles without inclusions. **(a)** Clean periods under $PM_{2.5}$ at 10 μg m^{-3}. **(b)** The high pollution level under $PM_{2.5}$ larger than 30 μg m^{-3}. **(c)** The median pollution level under $PM_{2.5}$ among 10–30 μg m^{-3}.

ACPD
15, 24369–24401, 2015

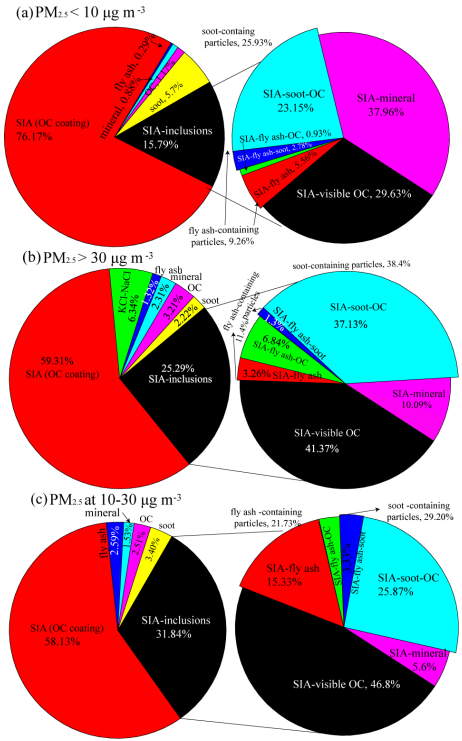

Figure 8. Identification of the pollution events based on individual particle analysis. **(a)** 684 individual particles and 108 SIA-inclusion particles, **(b)** 1214 individual particles and 307 SIA-inclusion particles. Eight samples were collected in $PM_{2.5}$ larger than 30 $\mu g\,m^{-3}$ induced by biomass burning emission. **(c)** 2355 individual particles and 750 SIA-inclusion particles. Nine samples were collected in $PM_{2.5}$ at the range of 10–30 $\mu g\,m^{-3}$ induced by biomass burning and industrial emissions. Four samples were collected in $PM_{2.5}$ smaller than 10 $\mu g\,m^{-3}$ which indicates clean period.

ACPD
15, 24369–24401, 2015

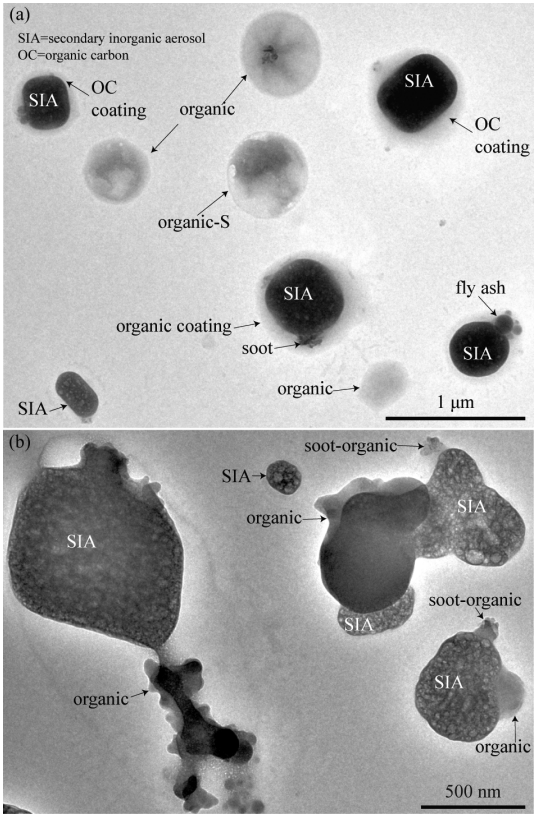

Figure 9. Individual particles during biomass burning periods with $PM_{2.5}$ mass concentration larger than 30 μg m^{-3}. **(a)** Organics and SIA-soot-(OC coating) particles on 12 October. **(b)** SIA-soot-(visible OC) on 19 October.

ACPD
15, 24369–24401, 2015

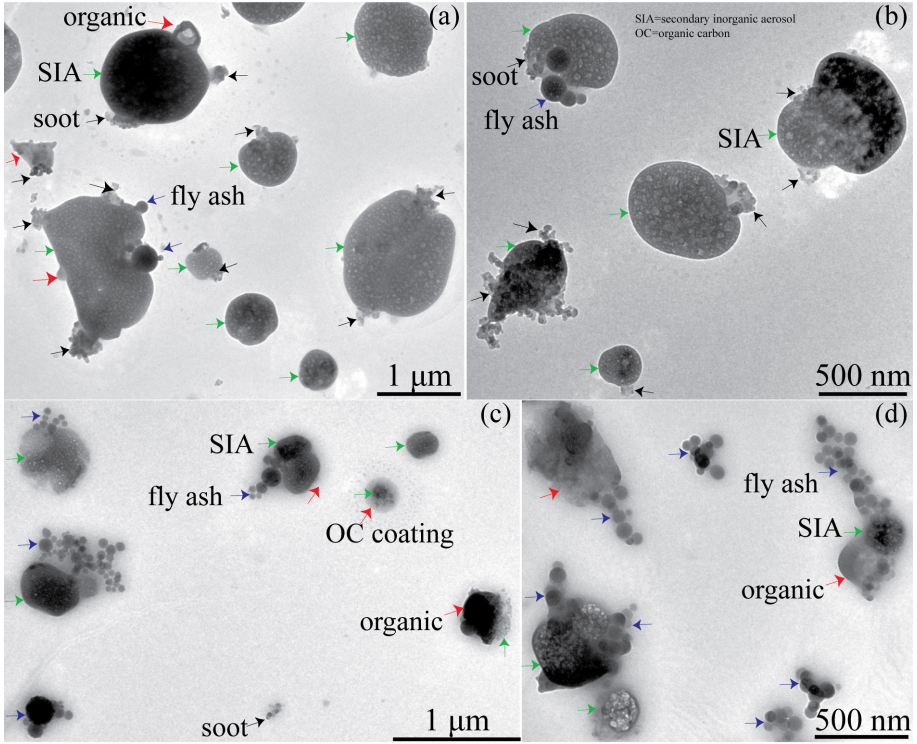

Figure 10. Individual particles collected under $PM_{2.5}$ mass concentration among 10–30 $\mu g\,m^{-3}$. **(a)** Mixture of SIA and soot, fly ash particles collected on 14 September. **(b)** Mixture of SIA and soot, fly ash particles collected on 18 September. **(c)** Mixture of SIA and fly ash, soot, organics collected on 29 September. **(d)** Mixing of SIA and fly ash, soot, organics collected on 10 October.

ACPD
15, 24369–24401, 2015